J Fluoresc (2014) 24:481–491
DOI 10.1007/s10895-013-1317-4

ORIGINAL PAPER

Unsymmetrically Substituted Nickel Triazatetra-Benzcorrole and Phthalocynanine Complexes: Conjugation to Quantum Dots and Applications as Fluorescent "Turn ON" Sensors

Oluwasesan Adegoke · Tebello Nyokong

Received: 13 August 2013 / Accepted: 9 October 2013 / Published online: 27 October 2013

Abstract We report on the design and application of fluorescent nanoprobes based on the covalent linking of $_L$-glutathione-capped CdSe@ZnS quantum dots (QDs) to newly synthesized unsymmetrically substituted nickel mercaptosuccinic acid triazatetra-benzcorrole (**3**) and phthalocyanine (**4**) complexes. Fluorescence quenching of the QDs occurred on conjugation to complexes **3** or **4**. The nanoprobes were selectively screened in the presence of different cations and Hg^{2+} showed excellent affinity in "turning ON" the fluorescence of the nanoprobes. Experimental results showed that the sensitivity of QDs-**4** towards Hg^{2+} was much higher than that of QDs-**3** nanoprobe. The mechanism of reaction has been elucidated based on the ability of Hg^{2+} to coordinate with the sulphur atom of the Ni complex ring and apparently "turn ON" the fluorescence of the linked QDs.

Keywords Phthalocyanine · Triazatetra-benzcorrole · Fluorescence enhancement · Quantum dots · Mercury

Introduction

The design and applications of quantum dots (QDs) in luminescence sensor technology have received considerable attention within the past decade [1–4]. Among numerous strategies [5–7] being employed to modify the surface of QDs in order to develop analytes-specific sensors, the coating with macrocylic compounds such as calixarene [8], cyclodextrin [9] crown ether [10] and porphyrins [11] is of significant interest. Most recently, development of new generation of nanosensors using metallophthalocyanine (MPc)-QDs conjugates has been the focus of research within our group [12–14]. The sensors work on the principle of a fluorescence "turn ON" mechanism in the presence of the target analyte.

While we have shown that symmetrically substituted MPc-QDs conjugates can be used for the fluorescence sensing of reactive oxygen species and anions [12–14], the use of QDs conjugates with unsymmetrically substituted MPc and triazatetra-benzcorrole (TBC) for analyte sensing has not been reported. The advantage of using unsymmetrical MPc is to ensure that only one reactive substituent of the MPc is conjugated to the QDs. On the other hand, TBCs are macrocylic compounds which have a similar structure to the Pc but their use in technological application has not been fully exploited. The only difference between Pc and TBC is that one of the bridging nitrogen atoms has been lost for the later [15]. To date, there have been no reports on the use of TBCs in optical sensor technology. Hence, a chemical sensing system based on QDs modified with TBC is employed in this work for the fluorescence recognition of analytes. TBCs display the signature UV-vis spectrum which has a significantly red-shifted Soret band (λ_{max}~450 nm) and a blue-shifted Q band compared to the corresponding phthalocyanine [16].

The complexes employed are: unsymmetrically substituted monomercaptosuccinic acid nickel phthalocyanine (complex **4**) and monomercaptosuccinic acid nickel triazatetra-benzcorrole (complex **3**). These complexes are conjugated to $_L$-glutathione (GSH)-capped CdSe@ZnS QDs for applications as fluorescence-based sensors. The use of mercaptosuccinic acid is to enable conjugation between the -COOH functional groups to the $-NH_2$ groups on the GSH capping of the CdSe@ZnS QDs. We have previously [13] shown that the nature of the central metal within the Pc ring is not important in the fluorescence "turn ON" by the analyte, hence Ni is employed as an example. In this work, the effect of the nature of the macrocyclic ring (Pc versus TBC) will be explored for the fluorescence recognition of analytes.

O. Adegoke · T. Nyokong (✉)
Department of Chemistry, Rhodes University, Grahamstown 6140, South Africa
e-mail: t.nyokong@ru.ac.za

The newly developed nanosensors were selectively screened in the presence of different cations (as discussed later) and the most selective cation (mercury) which induced an excellent fluorescence "turn ON" was chosen as the test ion. In addition, the toxicity of mercury ion in natural waters is a global concern [17]. Hence, developing a facile, rapid and highly sensitive method for its detection is of paramount importance.

Experimental

Materials

1-Ethyl-3-(3-dimethylaminopropyl)-carbodiimide (EDC), N-hydroxysuccinimide (NHS), trifluoroacetic acid (TFA), mercaptosuccinic acid (MSA), 1,2-dicyanobenzene, $NiCl_2.6H_2O$ and all metallic salts used in this work were obtained from Sigma-Aldrich. Methanol, acetone, tetrahydrofuran (THF), dimethylsulfoxide (DMSO) and dimethylformamide (DMF) were obtained from SAARCHEM. All chemicals were used as received. All solutions were prepared with ultra pure water obtained from a Milli-Q Water System (Millipore Corp. Bedford, MA, USA). All measurements for the detection of mercury ion were carried out in physiological conditions using 50 mM phosphate buffer solution (PBS) pH 7.4. The pH of the buffer solution was adjusted by addition of 1.0 M NaOH or HCl. The concentration of the QDs was determined using the extinction coefficients of CdSe QDs reported previously in literature [18]. Extinction coefficients when the QDs were linked to **3** and **4** were also determined using the same procedure [18].

Instrumentation

Excitation and emission spectra were recorded on a Varian Eclipse spectrofluorimeter. Ground state electronic absorption spectra were recorded on a Shimadzu UV-vis 2550 spectrophotometer. X-ray powder diffraction patterns were recorded using a Cu kα radiation ($\lambda = 1.5405$ Å, nickel filter), on a Bruker D8 Discover equipped with a proportional counter. A Metrohm Swiss 827 pH meter was used for pH measurements. FT-IR spectra were obtained on a Perkin-Elmer spectrum 100 with universal attenuated total reflectance (ATR) sampling accessory. Mass spectra data were collected with a Bruker AutoFLEX III Smart beam TOF/TOF Mass spectrometer. The spectra were acquired using α-cyano-4-hydroxycinnamic acid as the MALDI matrix, and a 355 nm Nd:YAG laser as the ionizing source. Elemental analyses were carried out on a Vario EL III MicroCube CHNS instrument analyzer. Energy dispersive spectroscopy (EDS) was carried out using an INCA PENTA FET coupled to a VAGA TESCAN using a 20 kV accelerating voltage. Transmission electron microscopy (TEM) images were obtained using a Zeiss Libra TEM 120 model operated at 90 kV. Fluorescence lifetime measurements were carried out using a time-correlated single photon counting (TCSPC) setup (FluoTime 200, Picoquant GmbH). The excitation source was a diode laser (LDH-P-C-485 with 10 MHz repetition rate, 88 ps pulse width and wavelength of 480 nm. Details have been provided before [12].

Synthesis

*4-Mercaptosuccinic Acid Phthalonitrile (**2**, Scheme 1)*

The synthesis of 4-nitrophthalonitrile (**1**) has previously been described [19]. Compound **2** was synthesized by reacting **1** (1.5 g, 8.4 mmol) and mercaptosuccinic acid (1.2 g, 8.0 mmol) in 15 mL of dry DMSO at room temperature under Ar atmosphere for 30 min. After this time, K_2CO_3 (4.6 g, 33.3 mmol) was added portion wise for 2 h. The reaction was allowed to stir and react for 24 h after which the product was washed several times with acetone, chloroform and diethyl ether.

Yield: 2.3 g, (96 %). IR [(ATR)°σ_{max}/cm^{-1}] 3324 (σ_{OH}), 2235 ($\sigma_{C=N}$), 1541–1650 ($\sigma_{C=O}$), 1345 (σ_{C-O}), 951 (σ_{C-S-C}). ^{1}H NMR (DMSO-d_6): δ, ppm 10.00 (1H, s, carboxy-H), 9.90 (1H, s, carboxy-H), 8.14 (3H, s, Ar-H), 4.02 (1H, s, methine-H), 2.50 (2H, s, methylene-H).

*Nickel Monomercaptosuccinic Acid Triazatetra-Benzcorrole (Scheme 1, (**3**))*

A mixture of $NiCl_2.6H_2O$ (0.34 g, 1.44 mmol), 4-mercaptosuccinic acid phthalonitrile (**2**) (0.25, 0.90 mmol), 1,2-dicyanobenzene (0.35 g, 2.7 mmol) and urea (0.30 g, 5 mmol) was stirred under Ar atmosphere in 20 mL of DMF at 180 °C for 1 h. After this time, the reaction temperature was lowered to 100 °C and the reaction allowed to continue for 24 h. After cooling, the crude product was washed sequentially with acetone, dichloromethane, hexane, THF:ammonia (1:1), chloroform:acetone (1:1) and diethylether. The desired product was then further purified using a Phenomenex C_{18} Sep-Pak column with a solvent mixture of chloroform:MeOH (2:1) to remove the undesired product followed by DMF:THF (10:1) with few drops of TFA to elute the desired complex.

Yield: 0.013 g (8 %). UV-vis (DMSO): λ_{max} (nm)(log ε) 673(4.11), 623(3.71), 598(3.66), 456(3.93), 404(3.93). IR [(ATR) σ_{max}/cm^{-1}] 3197 (σ_{OH}), 1532–1666 ($\sigma_{C=O}$), 1429 (σ_{C-OH}), 1334 (σ_{C-O}), 916 (σ_{C-S-C}), 755–800 (Ni-N). *Anal.* Calc. for $C_{36}H_{21}N_7O_4SNi.2H_2O$: C, 58.24; H, 3.37; N, 13.21. Found: C, 57.91; H, 3.24; N, 14.98. MALDI-TOF-MS *m/z:* Calc: 705.79. Found: 706.44 $[M]^-$ for $C_{36}H_{21}N_7O_4SNi$.

Scheme 1 Synthesis of 4-mercaptosuccinic acid phthalonitrile (**2**) and the corresponding **3** and **4** complexes

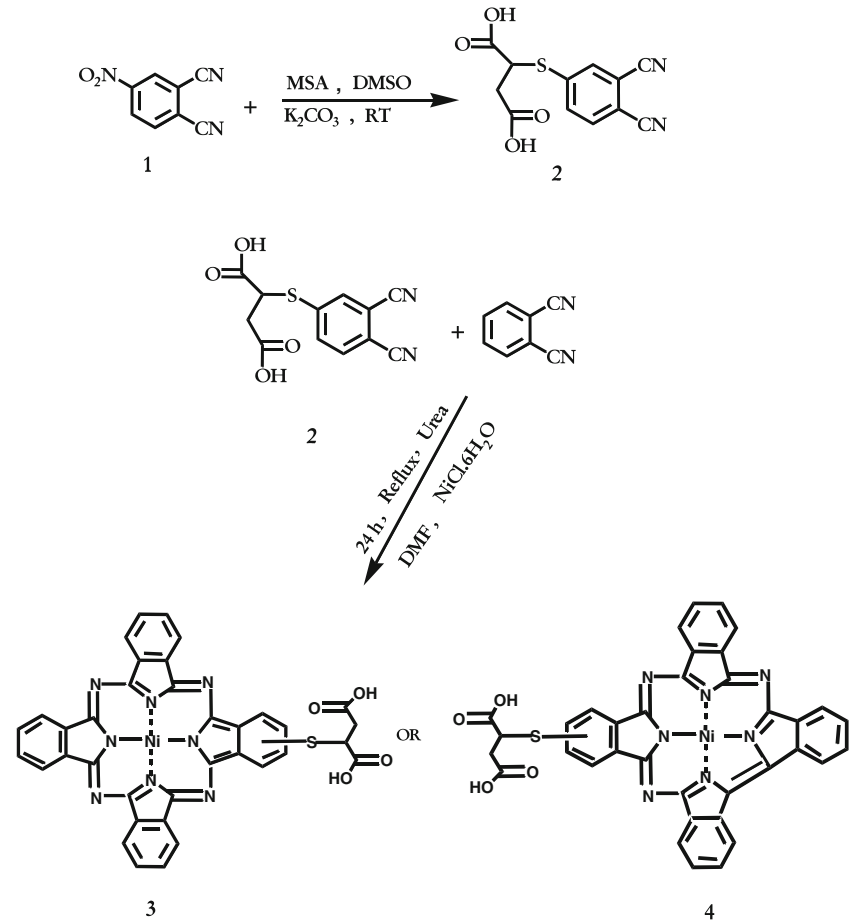

*Nickel Monomercaptosuccinic Acid Phthalocyanine (Scheme 1, (**4**))*

The synthesis and purification of **4** was the same for **3** except that the amount of urea used was 1.20 g (20 mmol). The amounts of all other reagents used was the same as that used for **3**. The desired product was eluted using a Phenomenex C_{18} Sep-Pak column with methanol:DMF (20:1) and few drops of TFA as eluent. Yield: 0.015 g (9 %). UV-vis (DMSO): λ_{max} (nm)(log ε) 672(4.70), 623(4.50), 588(4.45), 369(4.68). IR [(ATR) ν_{max}/cm^{-1}] 3024 (ν_{OH}), 1584–1649 ($\nu_{C=O}$), 1483 (ν_{C-OH}), 1332 (ν_{C-O}), 956 (ν_{C-S-C}), 752–828 (Ni-N). *Anal.* Calc. for $C_{36}H_{21}N_8O_4SNi.H_2O$: C, 58.55; H, 3.12; N 15.18. Found: C, 58.54; H, 3.23; N, 15.35. MALDI-TOF-MS *m/z:* Calc: 719.79. Found: 720.31 $[M]^-$ for $C_{36}H_{21}N_8O_4SNi$.

Conjugation of GSH-CdSe@ZnS QDs to **3** and **4** (Scheme 2)

CdSe@ZnS QDs were synthesized via previously described methods [20, 21] by capping with tri-n-octylphosphine oxide (TOPO) followed by ligand exchange with $_L$-glutathione (GSH).

The conjugation of GSH-CdSe@ZnS QDs to **3** and **4** was achieved following published procedures [12, 13] but with slight modifications. Briefly, aqueous solution of 0.1 M EDC (2 mL) was added to 1.5 mg each of **4** [5.7×10^{-5} M] and **3** [8.3×10^{-5} M] in DMSO:H_2O (3:2, v/v) to activate their corresponding carboxylic acid group. The solution was stirred for 24 h, then 10 mg of QDs in pH 7.4 PBS buffer (3 mL) was added followed by addition of 2 ml of aqueous solution of 0.1 M NHS and the reaction was allowed to proceed for another 24 h. The obtained linked QDs-**3** and QDs-**4** complexes were precipitated out from solution by the addition of methanol and centrifuged continuously to remove free QDs and also washed repeatedly with DMSO to remove unreacted Pc or TBC. Further purification of the conjugates was performed with the addition of methanol to ensure that the conjugate is completely free from unreacted QDs. The obtained conjugates were soluble in PBS buffer as a colloidal solution. It is important to note that the two terminal carboxylic groups of **3** and **4** could be coordinated to the QDs even though Scheme 2 displays the coordination of one terminal carboxylic group of the complexes to the QDs.

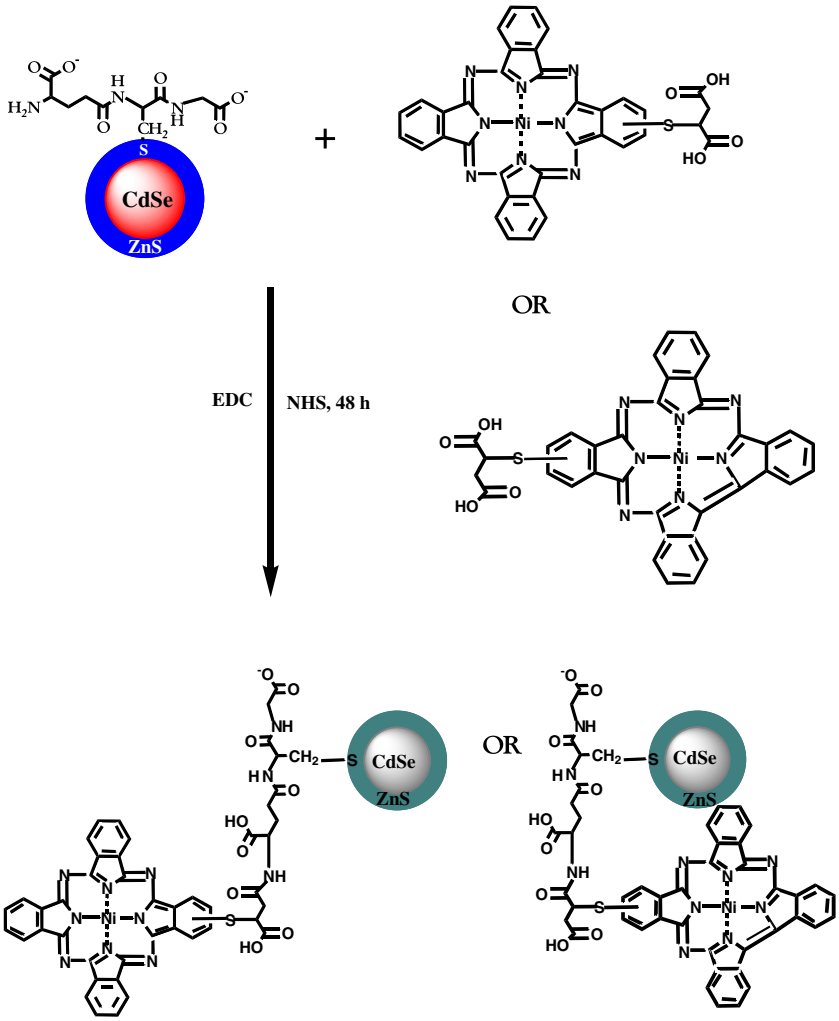

Scheme 2 Representation for the preparation of GSH-CdSe@ZnS-**4** and GSH-CdSe@ZnS-**3** nanoconjugates

Procedures for the Fluorimetric Detection of Mercury Ion in Aqueous Media

The obtained nanoconjugates were firstly dissolved in 3 mL of pH 7.4 buffer and ultrasonicated for 5 min to disperse the particles. Afterwards, different concentrations of Hg^{2+} (50 μl each) were added sequentially at intervals. In order to obtain a stable fluorescence signal, the fluorescence emission of the solution was measured after every 3 min of added Hg^{2+} concentration. An excitation wavelength of 500 nm was employed.

Results and Discussion

Characterization of Complexes **3** and **4**

The synthesis of complexes **3** and **4** occurred under similar conditions except that the amount of urea used was smaller for **3** than for **4**. Low amounts of urea resulted in the absence of one of the bridging nitrogen atoms and thus resulting in the formation of compound **3**. The synthesis of unsymmetrically substituted nickel mercaptosuccinic acid triazatetrabenzcorrole and phthalocyanine are reported here for the first time. Purification of unsymmetrically substituted Pcs is time consuming [22]. The same applies to TBCs. However, we successfully obtained complexes **3** and 4 after extensive washing with solvents and chromatographic separation. Even though symmetrically substituted metallo-triazatetrabenzcorrole are known [15, 23–25], the unsymmetrically substituted derivatives are reported here for the first time.

The complexes were characterized by UV/vis, FT-IR and MALDI TOF spectroscopies and by elemental analysis, all of which showed good agreements with the predicted structures as detailed in the experimental section.

The electronic spectra of the complexes measured before conjugation to the QD displayed a characteristic absorption in the Q band region with a maximum absorption wavelength of 673 nm for compound **3** and 672 nm for compound **4** in

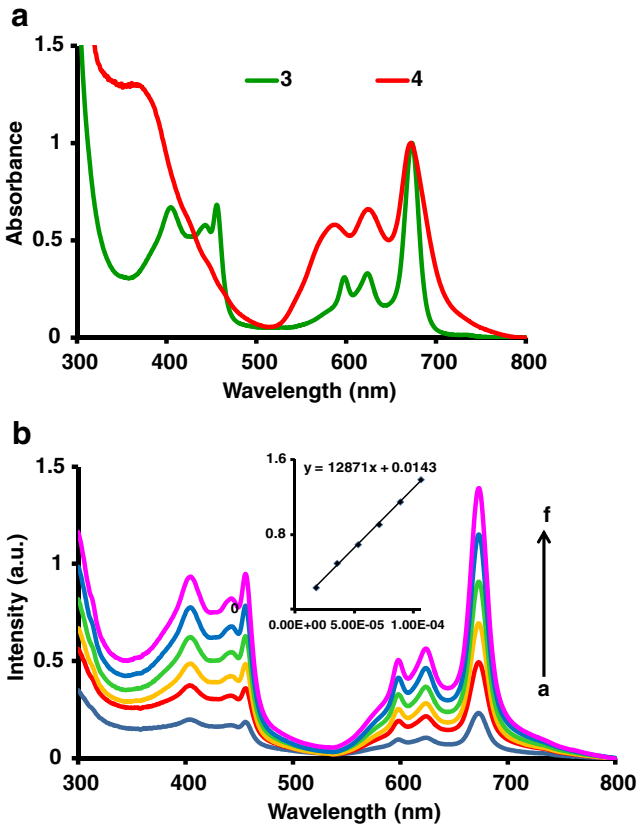

Fig. 1 **a** UV/vis absorption spectra of as-synthesized **3** and **4** in DMSO:H_2O (3:2, v/v). **b** Ground state absorption spectra of **3** at different concentration in DMSO showing that Beer-Lambert's law was obeyed. [3]=(a) 1.77×10^{-5}, (b) 3.54×10^{-5}, (c) 5.31×10^{-5}, (d) 7.08×10^{-5}, (e) 8.86×10^{-5}, (f) 1.06×10^{-4} M

DMSO:H_2O (3:2, v/v) as shown in Fig. 1a. The split Q band is due to unsymmetric substitution. Complex **3** displayed a split and broad Soret band between 404 and 456 nm. The sharp nature of the Soret band is characteristic of triazatetrabenzcorrole complexes [15, 24, 25]. We did not observe the blue shift in the Q band which has been observed on reduction of Pcs [16]. There was very little difference in the Q band maxima of **3** and **4**, Table 1. Figure 1b shows that Beer-Lambert's law was obeyed for compound **3** which was also observed for **4** (plot not shown).

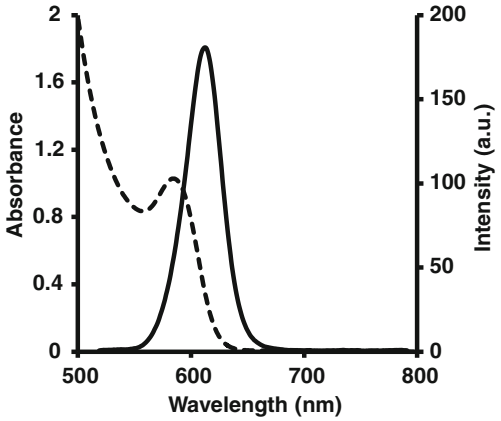

Fig. 2 Fluorescence emission (solid) and absorption (dotted line) of GSH-CdSe@ZnS QDs measured in 50 mM PBS buffer before conjugation. [3.0×10^{-6} M]

Characterization of GSH-CdSe@ZnS QDs

CdSe@ZnS QDs was chosen in this work due to its exceptional optical properties and was synthesized via the organometallic route. The wider band gap ZnS shell was coated on the surface of the core CdSe QDs to improve its photochemical properties. GSH (which contains a terminal amino group) was employed to obtain water-soluble QDs and also to allow for conjugation. As shown in Fig. 2, the QDs displayed a relatively symmetric and narrow emission spectrum with a maximum wavelength at 612 nm and an absorption peak at 584 nm in pH 7.4 buffer.

The fluorescence quantum yield (Φ_F) of the QDs was determined using established procedures [26] and the value obtained was 0.24, Table 1. The high value of Φ_F obtained for the QD strongly indicate a well passivated surface with the inorganic shell (ZnS) coating regardless of the ligand exchange step which is known [27] to decrease the fluorescent quantum yield.

X-ray powder diffraction (XRD) was employed to elucidate the size and crystal nature of the QDs. Figure 3 displays the XRD pattern for GSH-CdSe@ZnS QDs. The XRD pattern exhibit three characteristic peaks at $2\theta=26.2°$, 43.4° and 51.8° respectively. These correspond to (111), (220) and (311)

Table 1 Fluorescence lifetimes for a triexponential fit of GSH-CdSe@ZnS QDs, QDs-**3** and QDs-**4** nanoprobe in the absence and presence of Hg^{2+} in 50 mM PBS buffer, pH 7.4. Fret efficiencies, fluorescence quantum yields and LOD also included

QDs or conjugates	Eff	$\Phi_{F(QD)}$	Hg^{2+}[M]	τ_1 (ns)[a] ±0.1	τ_2 (ns)[a] ±0.06	τ_3 (ns)[a] ±0.02	Mean Life-time (ns)	LOD
GSH-CdSe@ZnS	–	0.24	–	19.1(0.58)	6.3(0.34)	1.3(0.8)	8.9	–
QDs-**3**	0.54	0.11	0	15.6(0.53)	4.5(0.37)	1.2(0.10)	7.1	2.0×10^{-10} M
			3.8×10^{-8}	18.2(0.53)	5.6(0.36)	1.3(0.11)	8.4	
QDs-**4**	0.75	0.06	0	14.7(0.52)	3.9(0.32)	1.2(0.16)	6.6	5.7×10^{-11} M
			3.8×10^{-8}	19.1(0.55)	6.3(0.36)	1.3(0.09)	8.9	

[a] Relative abundance in bracket

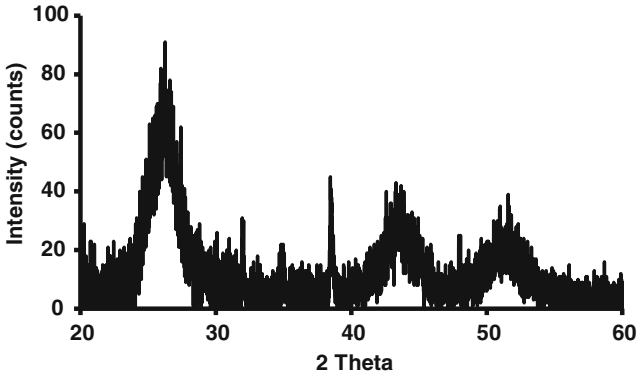

Fig. 3 XRD pattern for GSH-CdSe@ZnS QDs

planes of cubic CdSe (Joint Committee on Powder Diffraction Standards (JCPDS) No. 19–191) [28]. The average size of the QDs was estimated using the main XRD peak (111), according to the Scherrer Eq as previously reported [14]. The average particle size obtained was 4.7 nm.

Characterization of QDs-**3** and QDs-**4** Conjugates

TEM and EDS Measurements

In order to carry out morphological and structural elucidation of the QDs and their corresponding conjugates, TEM analysis was employed. Figure 4 shows the representative TEM images of the QDs alone (Fig. 4a), QDs-**3** (Fig. 4b) and QDs-**4** (Fig. 4c). For the QDs alone, it is clearly evident that the particle distributions are nearly mono-dispersed and spherical in shape. Upon conjugation to **3** or **4**, a more closed-packed particle morphology occurred, possibly due to the strong binding of the QDs to the Ni complexes.

Figure 4d shows the results of the EDS elemental analysis for QDs-**3** (as a representative of the two conjugates). From the observed EDS spectrum, the characteristic peaks of C, O, S, Cd, Ni, Zn and Se were present, confirming the formation of the conjugate. Among these elements, Cd, Se and Zn are

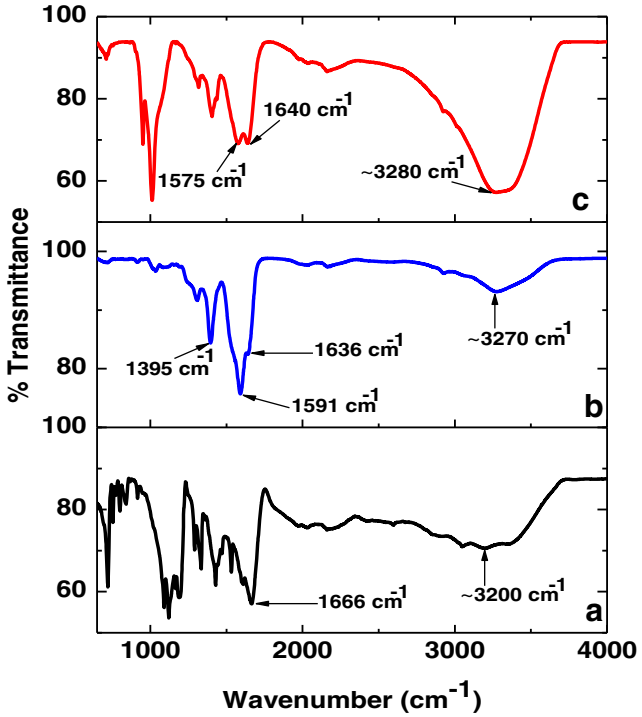

Fig. 5 FT-IR spectra of (a) **3**, (b) GSH-CdSe@ZnS QDs and (c) QDs-**3** used as a representative

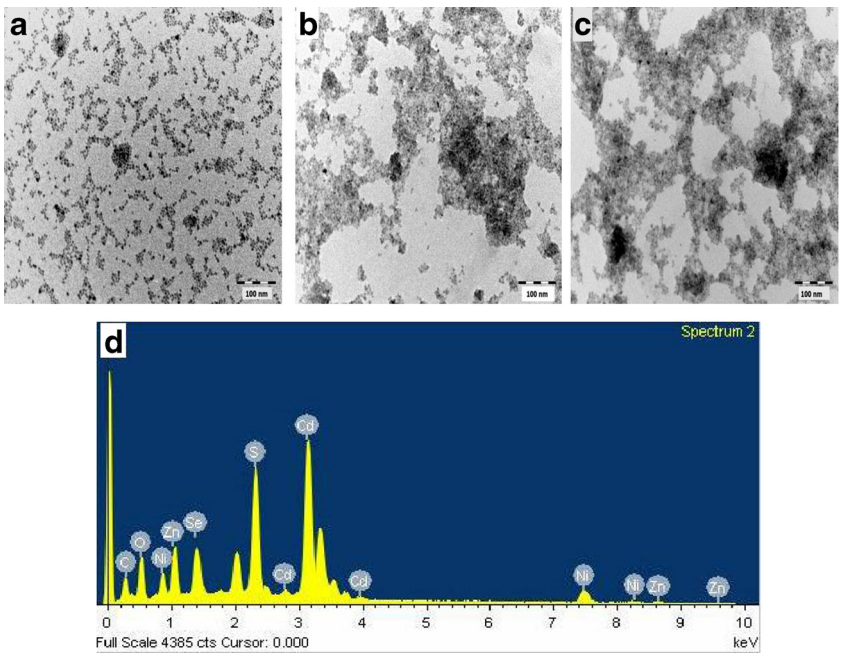

Fig. 4 TEM images of **a** GSH-CdSe@ZnS QDs, **b** QDs-**3** and **c** QDs-**4** nanoconjugates. **d** EDS spectrum of QDs-**3**

from the QDs, and Ni was from **3**. C, O and S are from both the QDs and complex **3**. In general, the results confirm that the QD was successfully conjugated to the Ni complex.

FT-IR Analysis

In order to confirm amide bond formation between the QDs and the Ni complexes, FT-IR analysis was carried out, Fig. 5. Complex **3** was chosen here as an example. Figure 5a shows the spectrum for **3** with the –C=O functional group appearing at 1666 cm^{-1} while the broad –OH functional group is depicted near 3200 cm^{-1}. For the QDs alone (Fig. 5b), the bands at 1395 and 1591 cm^{-1} may be related to the symmetric and asymmetric –COO group of GSH-CdSe@ZnS QDs, while the corresponding $–NH_2$ group appears near 3270 cm^{-1}. It is important to note that GSH contains an amide –CO-NH group, hence, the weak band at 1636 cm^{-1} can be attributed to the corresponding –CO-NH group. Figure 5c displays the FT-IR spectrum of the conjugate. The bands at 1575 and 1640 cm^{-1} are characteristics of the secondary and primary amide bonds [29] in the conjugate. In addition, the shift in IR bands is an indication of structural change [30]. Hence, the shift of the primary amide bond in the conjugate relative to GSH on the QDs may confirm the formation of such structural change. Also, the band at 3280 cm^{-1} for the conjugate may be assigned to the –NH functional group. It is important to note that the band in this region for the conjugate

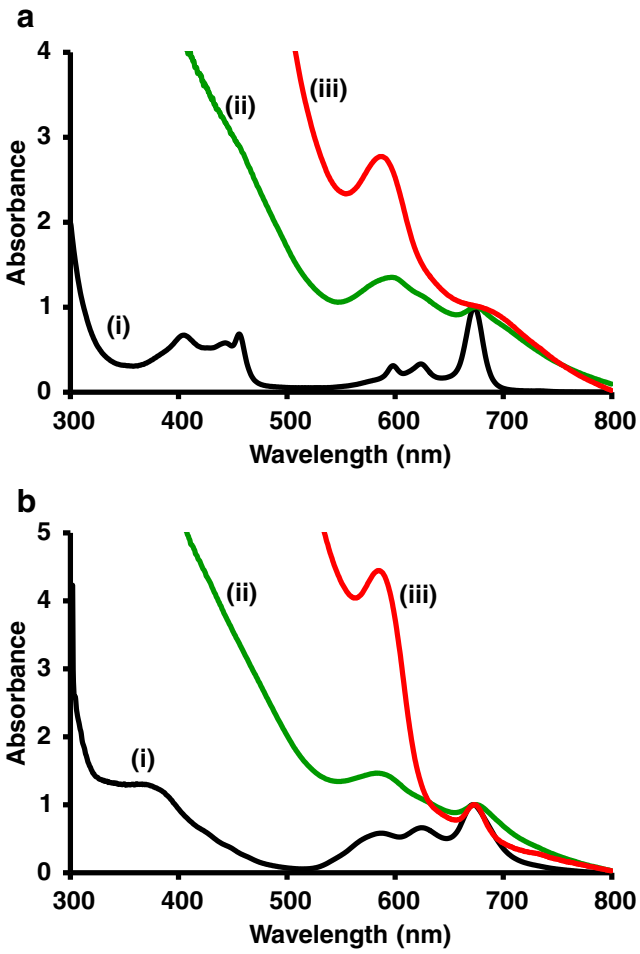

Fig. 6 UV/vis absorption spectra of **a 3** [8.3×10^{-5} M] and **b 4** [5.7×10^{-5} M] and their conjugates. (i) complexes **3** or **4** alone, (ii) QDs-**3** [7.4×10^{-6} M] or QDs-**4** [4.2×10^{-7} M] in DMSO:H_2O (3:2, v/v) and (iii) QDs-**3** [7.4×10^{-6} M] or QDs-**4** [4.2×10^{-7} M] in pH 7.4 PBS buffer

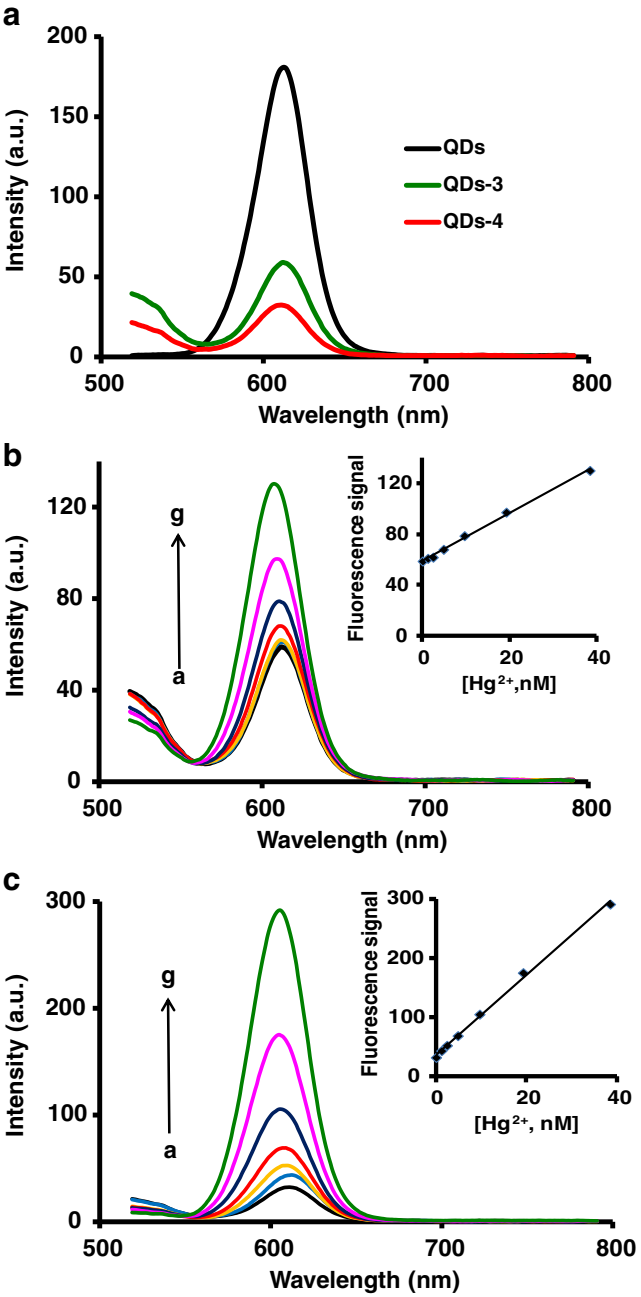

Fig. 7 Fluorescence emission spectra of **a** QDs alone, QDs-**3** and QDs-**4** conjugates; **b** QDs-**3** and (**c**) QDs-**4** upon addition of varying concentration of Hg^{2+}. For **b** and **c** inset=Plots of fluorescence signal versus Hg^{2+} concentration. [Hg^{2+}], a-g: 0, 1.2×10^{-9}, 2.4×10^{-9}, 4.8×10^{-9}, 9.6×10^{-9}, 1.9×10^{-8}, 3.8×10^{-8} M. Solvent=pH 7.4 buffer. λ_{exc}=500 nm

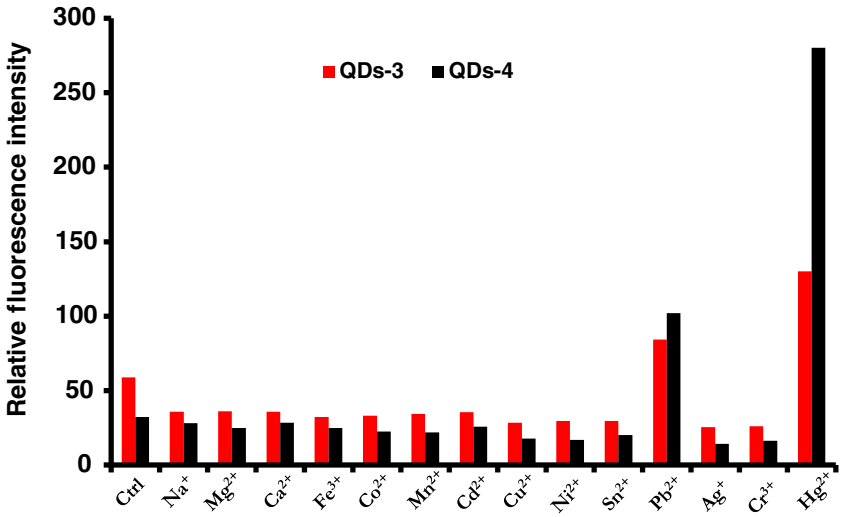

Fig. 8 Effects of different cations on the fluorescence response of QDs-**3** and QDs-**4** nanoprobe. Concentration of ions=8.0×10^{-8} M

(Fig. 5c) is more intense than that for the QDs alone (Fig. 5b) and the Ni complex (Fig. 5a). This gives an indication for the transformational change in the conjugate and hence the formation of the amide bond.

UV/vis Absorption Spectra

Figure 6 shows the UV/vis absorption spectra of **3** (Fig. 6a) and **4** (Fig. 6b) and their corresponding conjugates. For comparative purposes, the absorption spectra of the conjugates in Fig. 6a and b were measured in the same solvent medium (DMSO:H_2O (3:2, v/v)) employed to dissolve the complexes for conjugation to the QDs and also in pH 7.4 buffer used for the detection of analytes. It can be clearly observed that the absorption spectra of the conjugates both in DMSO:H_2O (3:2, v/v) and in pH 7.4 buffer displayed a combination of the absorption spectra of the Ni complexes and the QDs. There was more broadening of the Q band maxima of the QDs-**3** conjugate relative to QDs-**4** conjugate. In general, the observed features provide valuable information that the QDs have been successfully bonded to the Ni complexes.

Fluorescence Spectra and Parameters

Covalent binding of the QDs to the Ni complexes induced an apparent fluorescence "turn OFF" (quenching) of the QDs in the conjugates, Fig. 7a. The fluorescence quantum yields of the conjugate were determined using Eq. 1:

$$\Phi_{F(QD)}^{conjugate} = \Phi_{F(QD)} \frac{F_{QD}^{conjugate}}{F_{QD}} \quad (1)$$

where $F_{QD}^{conjugate}$ is the integrated fluorescence intensity of the QDs in the conjugates (QDs-**3** or QDs-**4**) and F_{QD} is the integrated fluorescence intensity of the QD alone. $\Phi_{F(QD)}$ (the fluorescence quantum yield of the QDs alone) was employed as the standard. As expected, the fluorescence quantum yield of QDs-**3** (Φ_F=0.11) and QDs-**4** (Φ_F=0.06) decreased relative to the value for the QDs alone (Φ_F=0.24), Table 1, which may be due to Förster resonance energy transfer (FRET) or other processes which deactivates the excited state of the QDs. FRET efficiencies (*Eff*) were evaluated from the fluorescence quantum yields, according to Eq. 2:

$$Eff = 1\frac{\Phi_{F(QD)}^{conjugate}}{\Phi_{F(QD)}} \quad (2)$$

The values obtained are 0.54 for QDs-**3** and 0.75 for QDs-**4**, Table 1. This implies that **4** have a greater prospect for energy transfer from the QDs than **3**.

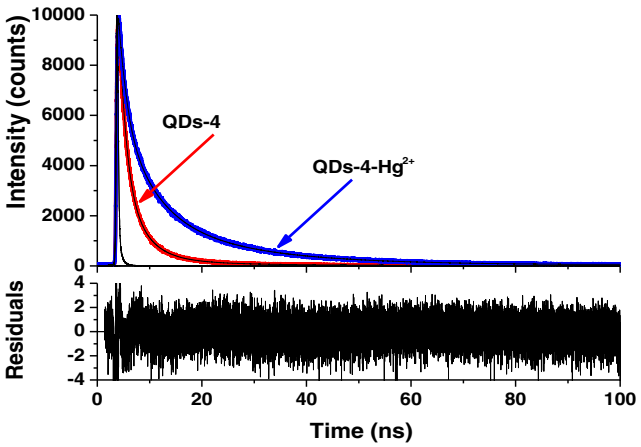

Fig. 9 Time-resolved fluorescence decay curve of QDs-**4** in the absence and upon addition of 3.8×10^{-8} M Hg^{2+}

Fluorescence Detection of Analytes

Selective Screening of Different Cations

The selective screening of different cations were performed using the proposed QDs-**3** and QDs-**4** nanoprobes. The following cations: Na^{+}, Mg^{2+}, Ca^{2+}, Fe^{3+}, Co^{2+}, Mn^{2+}, Cd^{2+}, Cu^{2+}, Ni^{2+}, Sn^{2+}, Pb^{2+}, Ag^{+}, Cr^{3+} and Hg^{2+} were examined at the same concentration level to determine their fluorescence response to the nanoprobe. A tolerable error of ±5.0 % in relative fluorescence intensity was taken into consideration. As shown in Fig. 8, Hg^{2+} induced a significant fluorescence "turn ON" of the sensor, while other cations further quenched the fluorescence except Pb^{2+}. The results imply that the proposed nanosensor can detect both Hg^{2+} and Pb^{2+} but with a greater sensitivity for the former than for the later. Hence, Hg^{2+} was selected as the ion of interest.

*Detection of Hg^{2+} Using the Proposed QDs-**3** and QDs-**4** Nanoprobes*

The fluorimetric detection of Hg^{2+} was performed using the proposed QDs-**3** and QDs-**4** nanoprobes in pH 7.4 buffer. The enhancement of quantum dots fluorescence on increasing concentration of Hg^{2+} is shown in Fig. 7a and b. The fluorescence signal increased linearly with the concentration of Hg^{2+} within the linear concentration range of 1.2×10^{-9} – 3.8×10^{-8} M. The limit of detection (LOD) was evaluated using the equation LOD=3 δ/K, where δ is the standard deviation of blank measurements ($n=10$) and K is the slope of the calibration curve. The LOD obtained were 2.0×10^{-10} M for QDs-**3** and 5.7×10^{-11} M for QDs-**4** nanoprobes, Table 1. This gives a good indication that **3** can be employed as molecular recognition sensor for ion sensing when coupled to QDs but with a much lower sensitivity as compared to QDs-**4** nanoprobe. Comparison of our proposed detection system with some

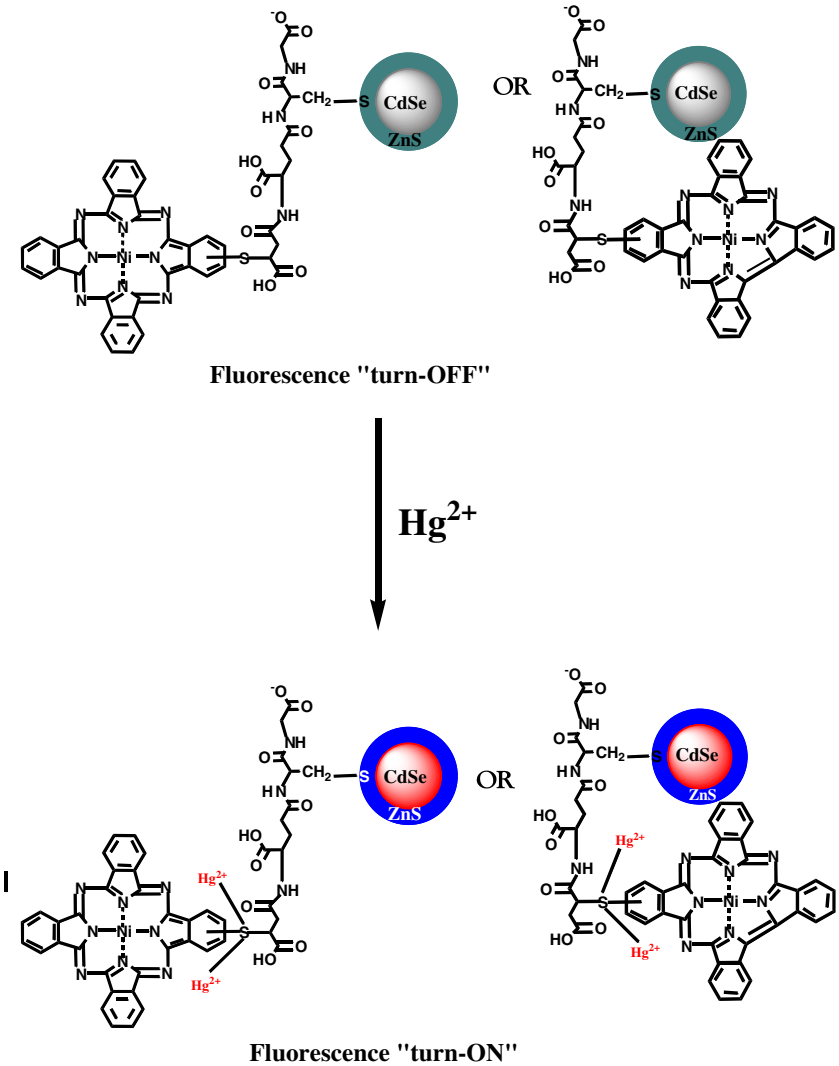

Scheme 3 Schematic representation for the detection mechanism of Hg^{2+} using the QDs-**3** and QDs-**4** nanoprobe

mercury-based QDs probes [31–34] showed an improvement in the detection sensitivity.

Time-Resolved Fluorescence Measurements

The fluorescence enhancement effect of Hg^{2+} on the proposed nanoprobe was further analyzed using time-resolved fluorescence measurements. Figure 9 shows fluorescence decay curves of QDs-**4** in the absence and presence of a known concentration of Hg^{2+}. A triexponential fluorescence lifetime was obtained as detailed in Table 1. The fitting of the luminescence decay curves for QDs or conjugates resulted in three lifetimes. The longer lifetime component τ_1 may be due to the involvement of surface states in the carrier recombination process [35], where the increase in radiative lifetime as a result of trapping of carrier states, by surface states, is a well-established feature [35]. The shortest component, τ_3 may be attributed to intrinsic recombination of initially populated core states. For ease of interpretation, the mean fluorescence lifetime was calculated. It was observed that the mean fluorescence lifetime of the conjugates decreased relative to the mean lifetime of the QDs alone. This may be due to FRET or other processes which quenched the fluorescence of the QDs on coordination to **3** and **4** as discussed above. In the presence of a known concentration of Hg^{2+}, the mean fluorescence lifetime of the conjugates increased and thus confirming the fluorescence "turn ON" effect of Hg^{2+} on the proposed nanoprobe. Hence, the observed fluorescence lifetime increase of the conjugate on interaction with Hg^{2+} can be interpreted as follows: the presence of Hg^{2+} blocked the non-radiative relaxation pathway which was associated with fluorescence quenching of the QDs on coordination to **3** or **4** and thus facilitated the radiative relaxation process of the QDs in the conjugate.

Proposed Mechanism for the Detection System

It has been reported before [36] that the QDs fluorescence emission is enhanced when the free motion of the surface substituents of the QDs is suppressed. This leads to an ordered orientation or improved rigidity of the surface substituent which could inhibit quenching of the QDs fluorescence and thus "turn ON" the fluorescence of the linked QDs. Hence, we propose that the fluorescence "turn ON" effect of Hg^{2+} on the proposed nanoprobe may be due to binding of Hg^{2+} to the sulfur groups anchored to the ring of **3** and **4**. The presence of the sulfur atoms on the Pc rings gives the opportunity to bind soft transition metal ions such as Ag^{+}, Pd^{2+}, Pb^{2+} and Hg^{2+} [37]. In fact, it has been demonstrated by Yangyang et al. [38] that Hg^{2+} specifically binds to sulfur groups of a cationic triazatetra-benzcorrole sensor. Hence, the same principle can be applied in this work as depicted in Scheme 3, in which Hg^{2+} binds specifically to the sulfur groups of the TBC or Pc ring and in turn influences the fluorescence "turn ON" mode of the QDs. Also, we propose that the differences in sensing abilities for Hg^{2+} compared to the other ions is related to its superior binding ability, which affects the motion of the Pc or TBC. Looking at Fig. 8, it shows that there is less enhance of fluorescence for complex **3** compared to 4, suggesting that the motion of the former is less affected by coordination of Hg^{2+} relative to 4.

Conclusions

We have synthesized for the first time unsymmetrical nickel mercaptosuccinic acid triazatetra-benzcorrole and phthalocyanine complexes and conjugated them to glutathione-capped CdSe@ZnS QDs for use as fluorescent nanoprobes. The proposed nanoprobes showed excellent affinity for detecting Hg^{2+} over other tested cations. The work presented here shows that both metallo-triaazatetra-benzcorrole and phthalocynanine complexes hold great promise as molecular recognition sensors when coordinated to QDs with the later showing a greater sensitivity.

Acknowledgments This work was supported by the Department of Science and Technology (DST) and National Research Foundation (NRF), South Africa through DST/NRF South African Research Chairs Initiative for Professor of Medicinal Chemistry and Nanotechnology as well as Rhodes University and DST/Mintek Nanotechnology Innovation Centre (NIC) – Sensors, South Africa.

References

1. Ji X, Zheng J, Xu J, Rastogi VK, Cheng T-C, DeFrank JJ, Leblanc RM (2005) (CdSe)ZnS Quantum dots and organophosphorus hydrolase bioconjugate as biosensors for detection of paraoxon. J Phys Chem B 109:3793–3799
2. Dezhurov SV, Volkova IY, Wakstein MS (2011) FRET-based biosensor for oleic acid in nanomolar range with quantum dots as an energy donor. Bioconjug Chem 22:338–345
3. Carrillo-Carrión C, Cárdenas S, Simonet BM, Valcárcel M (2009) Selective quantification of carnitine enantiomers using chiral cysteine-capped CdSe(ZnS) quantum dots. Anal Chem 81:4730–4733
4. Freeman R, Liu X, Willner I (2011) Amplified multiplexed analysis of DNA by the exonuclease III-catalyzed regeneration of the target DNA in the presence of functionalized semiconductor quantum dots. Nano Lett 11:4456–4461
5. Han B, Yuan J, Wang E (2009) Sensitive and selective sensor for biothiols in the cell based on the recovered fluorescence of the CdTe quantum dots-Hg(II) system. Anal Chem 81:5569–5573
6. Shi L, De Paoli V, Rosenzweig N, Rosenzweig Z (2006) Synthesis and application of quantum dots FRET-based protease sensors. J Am Chem Soc 128:10378–10379
7. Dubach JM, Harjes DI, Clark HA (2007) Ion-selective nano-optodes incorporating quantum dots. J Am Chem Soc 129:8418–8419

8. Jin T, Fujii F, Yamada E, Nodasaka Y, Kinjo M (2006) Control of the optical properties of quantum dots by surface coating with calix[n]arene carboxylic acids. J Am Chem Soc 128:9288–9289
9. Rakshit S, Vasudevan S (2008) Resonance energy transfer from beta-cyclodextrin-capped ZnO:MgO nanocrystals to included Nile Red guest molecules in aqueous media. ACS Nano 2:1473–1479
10. Chen C-Y, Cheng C-T, Lai C-W, Wu P-W, Wu K-C, Chou P-T, Chou Y-H, Chiu H-T (2006) Potassium ion recognition by 15-crown-5 functionalized CdSe/ZnS quantum dots in H_2O. Chem Commun 263–265
11. Frasco MF, Vamvakaki V, Chaniotakis N (2010) Porphyrin decorated CdSe quantum dots for direct fluorescent sensing of metal ions. J Nanoparticle Res 12:1449–1458
12. Adegoke O, Antunes E, Nyokong T (2013) Nanoconjugates of CdTe@ZnS quantum dots with cobalt tetraamino-phthalocyanine: Characterization and implications for the fluorescence recognition of superoxide anion. J Photochem Photobiol A Chem 257:11–19
13. Adegoke O, Khene S, Nyokong T (2013) Fluorescence "Switch on" of conjugates of CdTe@ZnS quantum dots with Al, Ni and Zn tetraamino-phthalocyanines by hydrogen peroxide: characterization and applications as luminescent nanosensors. J Fluoresc 23:963–974
14. Adegoke O, Nyokong T (2013) Fluorescence "turn on" probe for bromide ion using nanoconjugates of glutathione-capped CdTe@ZnS quantum dots with nickel tetraamino-phthalocyanine: characterization and size-dependent properties. J Photochem Photobiol A Chem 265: 58–66
15. Gouterman M, Sayer P, Shankland E, Smith JP (1981) Porphyrins. 41. Phosphorus mesoporphyrin and phthalocyanine. Inorg Chem 20(1):87–92
16. Gryko DT, Fox JP, Goldberg DP (2004) J Porphyrins Phthalocyanines 8:1091–1105
17. US EPA (2005) Regulatory impact analysis of the clean air mercury rule, EPA-452/R-05-003, Research Triangle Park, NC
18. Yu WW, Qu L, Guo W, Peng X (2003) Experimental determination of the extinction coefficient of CdTe, CdSe, and CdS nanocrystals. Chem Mater 2003(15):2854–2860
19. Wöhrle D, Eskes M, Shigehara K, Yamada A (1993) A simple synthesis of 4,5-disubstituted benzenes and octasubstituted phthalocyanines. Synthesis 194–196
20. Noh M, Kim T, Lee H, Kim C-K, Joo S-W, Lee K (2010) Fluorescence quenching caused by aggregation of water-soluble CdSe quantum dots. Colloids Surf A Physicochem Eng Asp 359:39–44
21. Dong W, Shen H-B, Liu X-H, Li M-J, Li L-S (2011) CdSe/ZnS quantum dots based fluorescence quenching method for determination of paeonol. Spectrochim Acta A 78:537–542
22. Chambrier, I, Cook MJ, Russell DA (1995) Synthesis and characterisation of functionalised phthalocyanine compounds for fabrication of self-assembled monolayers. Synthesis 1283–1286
23. Antunes EM, Nyokong T (2008) Synthesis and photophysical properties of tetra- and octasubstituted phosphorous oxide triazatetrabenzcorrole photosensitizers. Met Based Drugs. Article ID 498916
24. Song Z, Zhang F, Li X, Shek-Kiu C, Zhao F, Tang Y (2002) Investigation of a novel triazatetrabenzcorrole photosensitizer. J Porphyrins Phthalocyanines 6:484–488
25. Łapok L, Schnurpfeil G, Gerdes R, Gorun SM, Suvorova O, Kudryavtseva GS, Wöhrle D (2009) Synthesis of charged triazatetrabenzcorroles, phthalocyanines and tetrapyridylporphyrin, and their activities in the co-sensitized photooxidation of 2-mercaptoethanol. J Porphyrins Phthalocyanines 13:346–357
26. Fery-Forgues IS, Lavabre D (1999) Are fluorescence quantum yields so tricky to measure? A demonstration using familiar stationery products. J Chem Educ 76:1260–1264
27. Wang M, Felorzabihi N, Guerin G, Haley JC, Schole GD, Winnik MA (2007) Water-soluble CdSe quantum dots passivated by a multidentate diblock copolymer. Macromolecules 40:6377–6384
28. Chen S, Zhang X, Zhang Q, Hou X, Zhou Q, Yan J, Tan W (2011) CdSe quantum dots decorated by mercaptosuccinic acid as fluorescence probe for Cu^{2+}. J Lumin 131:947–951
29. Selim KMK, Xing Z, Choi M, Chang Y, Guo H, Kang I (2011) Reduced cytotoxicity of insulin-immobilized CdS quantum dots using PEG as a spacer. Nanoscale Res Lett 6:528–536
30. Cai X, Zhang Y, Zhang X, Jiang J (2006) Structures and properties of 2,3,9,10,16,17,23,24-octasubstituted phthalocyaninato-lead complexes: the substitutional effect study on the basis of density functional theory calculations. J Mol Struct THEOCHEM 801:71–80
31. Fang G, Xu M, Zeng F, Wu S (2010) β-cyclodextrin as the vehicle for forming ratiometric mercury ion sensor usable in aqueous media, biological fluids, and live cells. Langmuir 26:17764–17771
32. Lang AN, Wang L, Chen H-Q, Qian B-B, Ling B, Fu J (2010) Synchronous fluorescence determination of mercury ion with glutathione-capped CdS nanoparticles as a fluorescence probe. Talanta 81:438–443
33. Chao M-R, Chang Y-Z, Chen J-L (2013) Hydrophilic ionic liquid-passivated CdTe quantum dots for mercury ion detection. Biosens Bioelectron 42:397–402
34. Koneswaran M, Narayanaswamy R (2009) Mercaptoacetic acid capped CdS quantum dots as fluorescence single shot probe for mercury(II). Sensors Actuators B 139:91–96
35. Wang X, Qu L, Zhang J, Peng X, Xiao M (2003) Surface-related emission in highly luminescent CdSe quantum dots. Nano Lett 3:1103
36. Li H, Qu F (2007) Selective inclusion of polycyclic aromatic hydrocarbons (PAHs) on calixarene coated silica nanospheres englobed with CdTe nanocrystals. J Mater Chem 17:3536–3544
37. van Nostrum CF, Benneker FBG, Brussaard H, Kooijman H, Veldman N, Spek AL, Schoonman J, Feiters MC, Nolte RJM (1996) Dithiacrown ether substituted porphyrazines: synthesis, single-crystal structure, and control of aggregation in solution by complexation of transition-metal ions. Inorg Chem 35:959–969
38. Zhou Y, Deng M, Du Y, Yan S, Huang R, Weng X, Yang C, Zhang X, Zhou X (2011) A novel cationic triazatetrabenccorrole: selective detection of mercury(II) by nucleic acid-induced aggregation. Analyst 136:955–961